

YITP-SB-00-70
BNL-HET-00/42
RBRC-150
November 2000

Threshold Resummation and Rapidity Dependence

George Sterman^{a,b} and Werner Vogelsang^c

^a*C.N. Yang Institute for Theoretical Physics, SUNY Stony Brook
Stony Brook, New York 11794 – 3840, U.S.A.*

^b*Physics Department, Brookhaven National Laboratory,
Upton, NY 11973, U.S.A.*

^c*RIKEN-BNL Research Center, Bldg. 510a, Brookhaven National Laboratory,
Upton, New York 11973 – 5000, U.S.A.*

Abstract

We study the effects of threshold resummation on the rapidity dependence of single-particle-inclusive cross sections, using the prompt photon cross section as an example. We make use of the full resummation formula at next-to-leading logarithmic accuracy and develop a new technique for treating rapidity in resummation. We compare our phenomenological results with those of previous studies and discuss differences and similarities of the two existing resummation formalisms.

1 Introduction

Prompt-photon production at high transverse momentum [1], $pp, p\bar{p}, pN \rightarrow \gamma X$, has been a classic tool for constraining the nucleon’s gluon density, because at leading order a photon can be produced in the Compton reaction $qg \rightarrow \gamma q$. The “point-like” coupling of the photon to the quark provides a potentially clean electromagnetic probe of QCD hard scattering. A pattern of disagreement between theoretical predictions and experimental data for prompt photon production has been observed in recent years [2, 3, 4], however, not globally curable by changing the factorization and renormalization scales in the calculation, or by “fine-tuning” the gluon density [5, 6, 7]. The most serious problems relate to fixed-target data, where next-to-leading order (NLO) theory dramatically underpredicts some data sets [3, 4]. At collider energies [2], there is less reason for concern, but also here the agreement is not fully satisfactory. In this context, threshold resummations for the inclusive prompt photon cross section have been developed in [8, 9] and applied phenomenologically in [10, 11]. At partonic threshold when the initial partons have just enough energy to produce the high- p_T photon and a massless recoiling jet, the phase space available for gluon bremsstrahlung vanishes, resulting in logarithmic corrections to the partonic cross section. Threshold resummation [8, 9, 12, 13] organizes these corrections to all orders in α_s .

Phenomenological studies [10, 11] of threshold resummation for the prompt photon cross section have shown that the size of the resummation effects increases with $x_T \equiv 2p_T/\sqrt{S}$, where p_T is the photon transverse momentum. This is expected [8, 9] from the interplay of the resummed partonic cross section with steeply falling parton distributions, and explains why resummation effects are small for the prompt photon cross section measured at the Tevatron [2], where x_T is generally smaller than 0.1. In contrast to this, for fixed-target energies, where values as large as $x_T \approx 0.7$ are attained [3], a significant enhancement of the theory prediction was found. The enhancements found in [10, 11], however, are not sufficient to bring theory in line with all fixed-target data (or, of course, to reconcile conflicting data sets). Nonetheless, valuable insights have been gained from applying threshold resummation to the prompt photon cross section. One of them is that after resummation the theory predictions show a significant improvement in factorization and renormalization scale dependence [10] over NLO, which has a notoriously large scale sensitivity. This implies that threshold resummation does provide an important addition to the theory result, and has helped develop approaches [14, 15] that extend threshold resummation, by redistributing its contributions to the hard scattering function over soft gluon *transverse* momenta, giving rise to further enhancement of the cross section through recoil effects on the prompt photon spectrum.

We believe that further analyzing the effects of pure threshold resummation is useful, for two reasons. First, as mentioned above, threshold resummation for the prompt photon cross section has been carried out by two groups [8, 9]. Even though both results have been applied numerically [10, 11], a full comparison of the two formalisms has yet to be carried out, either

numerically, or at an analytical level. Indeed, it should be mentioned that there are genuine differences between the two formalisms: [8] resums at fixed, and arbitrary, photon rapidity, while [9] applies to the cross section fully integrated over rapidity. Therefore, it is interesting to compare the two approaches in cases where they both can be applied, which will show the close relation between the two.

Providing phenomenological results for the full content of the resummation formula of [8] is our other objective in this paper. In the numerical study of the inclusive cross section in [10], the full resummed expression of [9], which is at next-to-leading logarithmic (NLL) accuracy, was used, although rapidity acceptance was implemented indirectly, by adopting the angular dependence of NLO. In contrast, the analysis of [11], which made use of the formalism of [8], employed an expansion in the strong coupling truncated at next-to-next-to-leading order (NNLO). It is therefore interesting to study the role of higher-order terms, which do seem to have a fairly significant influence on the final result. To see how, we must develop a new practical technique for treating rapidity dependence in the resummed cross section, to which we will turn first in Sec. 2. This is an essential extension of the threshold resummation formalism, applicable to any resummed cross section at measured rapidity. Again, to make direct contact with the numerical studies of [10], we adopt the minimal prescription for moment inversion of [16].

In Sec. 3, we give explicit expressions for the resummation exponents at NLL accuracy, arising from the formalism of [8]. Section 4 presents the NLO hard-scattering functions that multiply the resummed exponents and collect contributions that are constant near threshold. The actual comparison between the two resummation formalisms of [8] and [9] is performed at an analytic level in Sec. 5. Section 6 discusses our treatment of the inverse Mellin and Fourier transforms required to obtain the physical cross section from the resummation formalism laid out in Sec. 2. Finally, in Sec. 7 we present numerical results for both resummation formalisms and provide phenomenological predictions for the prompt photon cross section resummed at fixed rapidity.

2 The resummed prompt-photon cross section

The cross section $p_T^3 d\sigma/dp_T d\eta$ for the single-inclusive production of a photon with transverse momentum p_T and pseudorapidity η is given in terms of the partonic cross section $p_T^3 d\hat{\sigma}/dp_T d\eta$ and the distribution functions $\phi_{a,b}$ for initial parton types a, b as

$$\frac{p_T^3 d\hat{\sigma}}{dp_T d\eta} = \sum_{a,b} \int_{x_a^{\min}}^1 dx_a \int_{x_b^{\min}}^1 dx_b \phi_a(x_a, \mu_F^2) \phi_b(x_b, \mu_F^2) \frac{p_T^3 d\hat{\sigma}_{ab}}{dp_T d\eta}(x_a P_A, x_b P_B, P_\gamma, \mu_F, \mu_R), \quad (1)$$

where P_A , P_B , P_γ are the momenta of the initial hadrons and the photon, and

$$x_a^{\min} = \frac{x_T e^\eta}{2 - x_T e^{-\eta}} \quad , \quad x_b^{\min} = \frac{x_a x_T e^{-\eta}}{2x_a - x_T e^\eta} \quad , \quad x_T = 2p_T/\sqrt{s}. \quad (2)$$

In Eq. (1), μ_F and μ_R denote the factorization and renormalization scales, respectively.

Threshold resummation is organized in Mellin- N moment space, where both the evolution of the parton densities and their convolution with the hard subprocess cross sections simplify. Were we interested simply in the cross section $d\sigma/dp_T$, integrated over all rapidities, an appropriate variable for taking moments would be x_T^2 , as shown in ref. [9]. If we wish to retain the rapidity dependence of the single-inclusive photon cross section $d\sigma/dp_T d\eta$, we need to introduce a double transform of the cross section. It turns out to be particularly convenient to do this by defining

$$\sigma(N, M) \equiv \frac{1}{\sqrt{2\pi}} \int_{-\infty}^{\infty} d\eta e^{iM\eta} \int_0^{1/\cosh^2 \eta} dx_T^2 \left(x_T^2\right)^{N-1} \frac{p_T^3 d\sigma}{dp_T d\eta}. \quad (3)$$

In this expression, we take Mellin moments in x_T^2 and a Fourier transform in rapidity. The latter makes use of the relation between the hadron and parton level center-of-mass system (c.m.s.) rapidities, η and $\hat{\eta}$, respectively:

$$\eta = \hat{\eta} + \frac{1}{2} \ln \left(\frac{x_a}{x_b} \right), \quad (4)$$

where x_a, x_b are the parton momentum fractions. Then, the Fourier phase factor $\exp(iM\eta)$ carries through to the parton level as $\exp(iM\hat{\eta}) x_a^{iM/2} x_b^{-iM/2}$, so that we will eventually arrive at a Fourier transform in partonic c.m.s. rapidity, along with shifts by $\pm iM/2$ in the complex plane of the Mellin moments of the parton distributions. Introducing the invariant mass of the unobserved hadronic final state,

$$s_4 = s(1 - \hat{x}_T \cosh \hat{\eta}), \quad (5)$$

where

$$s = x_a x_b S, \quad \hat{x}_T = \frac{x_T}{\sqrt{x_a x_b}}, \quad (6)$$

we indeed obtain

$$\begin{aligned} \sigma(N, M) &= \sqrt{\frac{2}{\pi}} \sum_{a,b} \tilde{\phi}_a^{N+1+\frac{iM}{2}} \tilde{\phi}_b^{N+1-\frac{iM}{2}} \int_{-\infty}^{\infty} d\hat{\eta} e^{iM\hat{\eta}} (\cosh \hat{\eta})^{-2N} \int_0^s \frac{ds_4}{s} \left(1 - \frac{s_4}{s}\right)^{2N-1} \frac{p_T^3 d\hat{\sigma}_{ab}}{dp_T d\hat{\eta}} \\ &\equiv \frac{1}{\sqrt{2\pi}} \sum_{a,b} \tilde{\phi}_a^{N+1+\frac{iM}{2}} \tilde{\phi}_b^{N+1-\frac{iM}{2}} \int_{-\infty}^{\infty} d\hat{\eta} e^{iM\hat{\eta}} (\cosh \hat{\eta})^{-2N} \tilde{\omega}_{ab}(2N, \hat{\eta}). \end{aligned} \quad (7)$$

The second relation serves as the definition of the hard-scattering function $\tilde{\omega}_{ab}$, in Mellin-moment space, as a function of rapidity. Moments of the parton distributions are denoted by

$$\tilde{\phi}_a^L \equiv \int_0^1 dx x^{L-1} \phi_a(x, \mu_F^2). \quad (8)$$

Threshold resummation for the single-particle inclusive cross section organizes corrections as singular as $\alpha_s^n [\ln^m(s_4/s)/s_4]_+$, $m \leq 2n-1$, near partonic threshold, $s_4 \rightarrow 0$, to all orders in perturbation theory. Let us define by $N' \equiv 2N$ the moment variable conjugate to $(1 - s_4/s)$. This variable was denoted as N in Ref. [8]. In Mellin- N' space, these logarithms translate into terms of the form $\alpha_s^n \ln^m(N')$, $m \leq 2n$. The hard scattering functions $\tilde{\omega}_{ab}(N', \hat{\eta})$ for qg and $q\bar{q}$

scattering, resummed to NLL accuracy at *fixed* rapidity $\hat{\eta}$, were derived in [8], and are given as

$$\begin{aligned}\tilde{\omega}_{ab}(N', \hat{\eta}) &= \alpha \alpha_s(\mu_R^2) C_{ab}(\hat{\eta}, \alpha_s(\mu_R^2)) \exp\{E'_c(N', s)\} \exp\left\{\sum_{i=a,b} E_i(N'_i, s)\right\} \\ &\times \exp\left[\int_{\mu_R}^{\sqrt{s}/N'} \frac{d\mu'}{\mu'} 2 \operatorname{Re}\Gamma_S^{(ab \rightarrow \gamma c)}(\hat{\eta}, \alpha_s(\mu'^2))\right],\end{aligned}\quad (9)$$

with $N'_i = 2N_i$, $N_a = N(-u/s)$, $N_b = N(-t/s)$. We now describe each of these functions, starting from the left. The coefficients $C_{ab}(\hat{\eta}, \alpha_s)$ include the underlying Born $2 \rightarrow 2$ hard scatterings $ab \rightarrow \gamma c$, and also absorb factors in the cross section that are constant in the large- N' limit at fixed $\hat{\eta}$, produced by hard virtual and non-logarithmic soft higher-order contributions [9]. The C_{ab} are subject to $2 \rightarrow 2$ kinematics, with $\hat{x}_T = 1/\cosh(\hat{\eta})$, and are functions of $\hat{\eta}$ and the strong coupling only,

$$C_{ab}(\hat{\eta}, \alpha_s) = \sum_{n=0}^{\infty} \left(\frac{\alpha_s}{\pi}\right)^n C_{ab}^{(n)}(\hat{\eta}). \quad (10)$$

Their leading terms $C_{ab}^{(0)}$ are just the $2 \rightarrow 2$ cross sections for $ab \rightarrow \gamma c$, given in our normalization by

$$\begin{aligned}C_{q\bar{q}}^{(0)}(\hat{\eta}) &= \frac{\pi e_q^2 C_F}{C_A} \frac{1}{2 \cosh^4(\hat{\eta})} \left(\frac{t}{u} + \frac{u}{t}\right), \\ C_{qg}^{(0)}(\hat{\eta}) &= \frac{\pi e_q^2}{2C_A} \frac{1}{2 \cosh^4(\hat{\eta})} \left(-\frac{t}{s} - \frac{s}{t}\right),\end{aligned}\quad (11)$$

where $t = (p_a - p_\gamma)^2 = -s \hat{x}_T e^{-\hat{\eta}}/2$, $u = (p_b - p_\gamma)^2 = -s \hat{x}_T e^{\hat{\eta}}/2$. The next-order terms $C_{ab}^{(1)}$ can be extracted explicitly [9] from the complete NLO calculation of [17]; see below.

To the right of the coefficient functions C_{ab} in Eq. (9), each of the exponential factors is associated with one of the sets of on-shell quanta that characterize the hard-scattering process near partonic threshold. These are: quanta collinear to the incoming partons, quanta collinear to the final-state jet that recoils against the photon, and soft-gluon radiation.

The resummed exponents for the initial state partons in Eq. (9) are given by

$$\begin{aligned}E_i(2N_i, M_i) &= -\int_0^1 dz \frac{z^{2N_i-1} - 1}{1-z} \left\{ \int_{(1-z)^2}^1 \frac{dt}{t} A_i \left[\alpha_s(t M_i^2) \right] + \bar{B}_i \left(\nu_i, \frac{M_i^2}{s}, \alpha_s((1-z)^2 M_i^2) \right) \right\} \\ &\quad - 2 \int_{\mu_R}^{M_i} \frac{d\mu'}{\mu'} \gamma_i \left(\alpha_s(\mu'^2) \right) + 2 \int_{\mu_F}^{M_i} \frac{d\mu'}{\mu'} \gamma_{ii} \left(2N_i, \alpha_s(\mu'^2) \right),\end{aligned}\quad (12)$$

where M_i is a scale of order \sqrt{s} . As we shall see, the exponent is actually independent of M_i to NLL. In addition,

$$\begin{aligned}A_i(\alpha_s) &= C_i \left(\frac{\alpha_s}{\pi} + \frac{1}{2} K \left(\frac{\alpha_s}{\pi} \right)^2 \right), \quad K = C_A \left(\frac{67}{18} - \frac{\pi^2}{6} \right) - \frac{5}{9} n_f, \\ \bar{B}_i \left(\nu_i, \frac{M_i^2}{s}, \alpha_s \right) &= C_i \frac{\alpha_s}{\pi} \left[1 - \ln(2\nu_i) + \ln \left(\frac{M_i^2}{s} \right) \right].\end{aligned}\quad (13)$$

Here, $C_q = C_F = 4/3$ and $C_g = C_A = 3$, and n_f is the number of flavors. The ν_i contain the gauge dependence, introduced to define the factorized cross section [8],

$$\nu_i \equiv \frac{(\beta_i \cdot n)^2}{|n^2|}. \quad (14)$$

where $\beta_i^\mu = p_i^\mu \sqrt{2/s}$, and n an axial gauge vector. Furthermore, to one loop order

$$\begin{aligned} \gamma_q(\alpha_s) &= \frac{3}{4} C_F \frac{\alpha_s}{\pi}, & \gamma_{qq}(N, \alpha_s) &= -\left(\ln N - \frac{3}{4}\right) C_F \frac{\alpha_s}{\pi}, \\ \gamma_g(\alpha_s) &= b_0 \alpha_s, & \gamma_{gg}(N, \alpha_s) &= -(C_A \ln N - \pi b_0) \frac{\alpha_s}{\pi}, \end{aligned} \quad (15)$$

where $b_0 = (11C_A - 4T_R n_f)/(12\pi)$, with $T_R = 1/2$, and where $\bar{N} \equiv N e^{\gamma_E}$, with γ_E the Euler constant. The γ_i are the anomalous dimensions of the quark and gluon fields, and the γ_{ii} the $\ln N$ and constant terms in the negative of the moments of the diagonal splitting functions. As can be seen from (9), they organize renormalization- and factorization-scale dependence, respectively.

The four terms in the initial-state exponent are closely linked by the relation between the large- N behavior of diagonal splitting functions and anomalous dimensions,

$$\gamma_{ii}(N, \alpha_s) = -\ln \bar{N} A_i(\alpha_s) + \gamma_i(\alpha_s), \quad (16)$$

where, as above, $\bar{N} = N e^{\gamma_E}$. Each of the four terms in E_i plays a specific role in the resummation process. The first, double-integral, term organizes double-logarithmic behavior associated with soft and collinear divergences in terms of the universal behavior of splitting functions. The second, single-logarithmic, term matches the behavior of the splitting functions to that of the physical cross section, factorized as in Ref. [8]. The third term summarizes noneikonal logarithms in virtual diagrams, while the fourth matches large transverse momentum subtractions associated with the $\overline{\text{MS}}$ scheme to the double-logarithmic term. Using Eq. (16), we readily show that at NLL, E_i is independent of the M_i . In our notation, Refs. [8] and [11] adopt the choices $M_a = -u/\sqrt{s}$ and $M_b = -t/\sqrt{s}$.

From the final-state jet that recoils against the photon, one has the exponent

$$\begin{aligned} E'_c(2N, s) &= \int_0^1 dz \frac{z^{2N-1} - 1}{1-z} \left\{ \int_{(1-z)^2}^{(1-z)} \frac{dt}{t} A_c[\alpha_s(ts)] - \gamma_c[\alpha_s((1-z)s)] \right. \\ &\quad \left. - \bar{B}_c[\nu_c, 1, \alpha_s((1-z)^2 s)] \right\} + 2 \int_{\mu_R}^{\sqrt{s}} \frac{d\mu'}{\mu'} \gamma_c(\alpha_s(\mu'^2)), \end{aligned} \quad (17)$$

where \bar{B}_c is defined in Eq. (13) above. As for the initial-state jet, the A_c and \bar{B}_c terms may be associated with the eikonal approximation, while the γ_c terms organize the remaining, collinear logarithms. Again, compared to Ref. [8], we make the dependence on the renormalization scale explicit, although it is not associated with logarithms of the moment variable.

The final factor in Eq. (9) resums NLL terms from coherent soft gluon emission between the jets. The rapidity-dependent anomalous dimension governing this soft radiation depends on the flavor combination in the hard scattering. For the process $q\bar{q} \rightarrow \gamma g$, it is given by

$$\Gamma_S^{(q\bar{q} \rightarrow \gamma g)}(\hat{\eta}, \alpha_s) = \frac{\alpha_s}{2\pi} \left\{ C_F [-\ln(4\nu_q \nu_{\bar{q}}) + 2 - 2\pi i] + C_A \left[\ln\left(\frac{tu}{s^2}\right) + 1 - \ln(2\nu_g) + \pi i \right] \right\}. \quad (18)$$

For the process $qg \rightarrow \gamma q$, it reads

$$\Gamma_S^{(qg \rightarrow \gamma q)}(\hat{\eta}, \alpha_s) = \frac{\alpha_s}{2\pi} \left\{ C_F \left[2 \ln\left(\frac{-u}{s}\right) - \ln(4\nu_{qa} \nu_{qc}) + 2 \right] + C_A \left[\ln\left(\frac{t}{u}\right) - \ln(2\nu_g) + 1 - \pi i \right] \right\}. \quad (19)$$

Note that the dependence on the gauge vector n in all these expressions, contained in the ν_i , Eq. (14), drops out when all contributions to Eq. (9) are combined [8, 11, 18]. Indeed, by redefining the soft and jet functions as in Refs. [14], we may eliminate this dependence at the beginning. Here, however, we retain it, again for ease of comparison to Refs. [8] and [11].

3 NLL exponents

Following the procedures of [9, 20], we reexpress the three exponents in Eq. (9) in a form with NLL accuracy. The respective results for each exponent are given in Appendix A. The sources of $\hat{\eta}$ dependence are readily visible from the expressions given there and are: the dependence of the initial-state exponents E_i on $\lambda_i \equiv \alpha_s b_0 \ln N_i$ (where $\alpha_s \equiv \alpha_s(\mu_R^2)$), the dependence of the final-state jet function on $s = 4p_T^2 \cosh^2 \hat{\eta}$, and the dependence of the soft anomalous dimensions $\Gamma_S^{(ab \rightarrow \gamma c)}$ on the subprocess Mandelstam variables s, t, u , as given above. After combining all NLL exponents given in Appendix B, we find that for both partonic channels the $\hat{\eta}$ dependence is purely of the form $\ln(\cosh \hat{\eta})$:

$$\begin{aligned} & (\alpha_s \alpha_s)^{-1} \int_{-\infty}^{\infty} d\hat{\eta} e^{iM\hat{\eta}} (\cosh \hat{\eta})^{-2N} \tilde{\omega}_{ab}(2N, \hat{\eta}) \\ &= \int_{-\infty}^{\infty} d\hat{\eta} e^{iM\hat{\eta}} (\cosh \hat{\eta})^{-2N} C_{ab}(\hat{\eta}, \alpha_s) \exp \left[\ln \tilde{N} g_{ab}^{(1)}(\tilde{\lambda}) + g_{ab}^{(2)} \left(\tilde{\lambda}, \frac{Q^2}{\mu_R^2}, \frac{Q^2}{\mu_F^2} \right) + \ln(\cosh \hat{\eta}) g_{ab}^{(3)}(\tilde{\lambda}) \right] \\ &= \exp \left[\ln \tilde{N} g_{ab}^{(1)}(\tilde{\lambda}) + g_{ab}^{(2)} \left(\tilde{\lambda}, \frac{Q^2}{\mu_R^2}, \frac{Q^2}{\mu_F^2} \right) \right] \int_{-\infty}^{\infty} d\hat{\eta} e^{iM\hat{\eta}} (\cosh \hat{\eta})^{-2N + g_{ab}^{(3)}(\tilde{\lambda})} \left[C_{ab}^{(0)}(\hat{\eta}) + \frac{\alpha_s}{\pi} C_{ab}^{(1)}(\hat{\eta}) \right], \end{aligned} \quad (20)$$

where $Q^2 \equiv 2p_T^2$, and $\tilde{N} \equiv N+1$, $\tilde{\lambda} \equiv \alpha_s b_0 \ln(N+1)$. Here we have adopted the convention of [9] to evaluate the resummation exponents at the moment variable $N+1$, rather than at N , since the former naturally appears in the moments of the parton densities; see Eq. (7) and Eqs. (32), (33) below. The functions $g_{ab}^{(1)}(\lambda)$ and $g_{ab}^{(2)}(\lambda, Q^2/\mu_R^2, Q^2/\mu_F^2)$ (where $\lambda \equiv \alpha_s b_0 \ln N$) resum LL and NLL terms, respectively, that are independent of $\hat{\eta}$. Resummation of the $\hat{\eta}$ dependence is taken care of by the functions $g_{ab}^{(3)}(\lambda)$, which are of NLL order only. The particular simplicity of the $\hat{\eta}$ dependence in the exponent makes it possible to join all $g_{ab}^{(3)}$ terms with the moment variable in the $\hat{\eta}$ integrand.

The functions $g_{ab}^{(1)}(\lambda)$ and $g_{ab}^{(2)}(\lambda, Q^2/\mu_R^2, Q^2/\mu_F^2)$ have already been presented in [9], and we recall them here:

$$\begin{aligned} g_{q\bar{q}}^{(1)}(\lambda) &= (2C_F - C_A) h^{(1)}(\lambda) + C_A h^{(1)}(\lambda/2) , \\ g_{qg}^{(1)}(\lambda) &= C_A h^{(1)}(\lambda) + C_F h^{(1)}(\lambda/2) , \end{aligned} \quad (21)$$

where

$$h^{(1)}(\lambda) = \frac{1}{2\pi b_0 \lambda} \left[2\lambda + (1-2\lambda) \ln(1-2\lambda) \right] , \quad (22)$$

while,

$$\begin{aligned} g_{q\bar{q}}^{(2)}\left(\lambda, \frac{Q^2}{\mu_R^2}, \frac{Q^2}{\mu_F^2}\right) &= (2C_F - C_A) h^{(2)}(\lambda) + 2C_A h^{(2)}(\lambda/2) \\ &+ \frac{2C_F - C_A}{2\pi b_0} \ln 2 \ln(1-2\lambda) + \frac{C_A \gamma_E - \pi b_0}{\pi b_0} \ln(1-\lambda) - \frac{2C_F}{\pi b_0} \lambda \ln \frac{Q^2}{\mu_F^2} \\ &+ \left\{ \frac{C_F}{\pi b_0} [2\lambda + \ln(1-2\lambda)] + \frac{C_A}{2\pi b_0} [2 \ln(1-\lambda) - \ln(1-2\lambda)] \right\} \ln \frac{Q^2}{\mu_R^2} , \end{aligned} \quad (23)$$

$$\begin{aligned} g_{qg}^{(2)}\left(\lambda, \frac{Q^2}{\mu_R^2}, \frac{Q^2}{\mu_F^2}\right) &= C_A h^{(2)}(\lambda) + 2C_F h^{(2)}(\lambda/2) \\ &+ \frac{C_A}{2\pi b_0} \ln 2 \ln(1-2\lambda) + \frac{4C_F \gamma_E - 3C_F}{4\pi b_0} \ln(1-\lambda) - \frac{C_F + C_A}{\pi b_0} \lambda \ln \frac{Q^2}{\mu_F^2} \\ &+ \left\{ \frac{C_F + C_A}{2\pi b_0} [2\lambda + \ln(1-2\lambda)] + \frac{C_F}{2\pi b_0} [2 \ln(1-\lambda) - \ln(1-2\lambda)] \right\} \ln \frac{Q^2}{\mu_R^2} , \end{aligned} \quad (24)$$

where $Q^2 = 2p_T^2$, γ_E is the Euler constant, $\gamma_E = 0.5772\dots$, and

$$h^{(2)}(\lambda) = \frac{b_1}{2\pi b_0^3} \left[2\lambda + \ln(1-2\lambda) + \frac{1}{2} \ln^2(1-2\lambda) \right] - \frac{\gamma_E}{\pi b_0} \ln(1-2\lambda) - \frac{K}{4\pi^2 b_0^2} \left[2\lambda + \ln(1-2\lambda) \right] , \quad (25)$$

with $b_1 = (17C_A^2 - 10C_A T_R n_f - 6C_F T_R n_f)/(24\pi^2)$. The coefficient K has already been defined in (13). The functions $g_{ab}^{(3)}(\lambda)$ are new to this analysis and read

$$\begin{aligned} g_{q\bar{q}}^{(3)}(\lambda) &= (2C_F - C_A) h^{(3)}(\lambda) + C_A h^{(3)}(\lambda/2) , \\ g_{qg}^{(3)}(\lambda) &= C_A h^{(3)}(\lambda) + C_F h^{(3)}(\lambda/2) , \end{aligned} \quad (26)$$

where

$$h^{(3)}(\lambda) = \frac{2}{\pi b_0} \ln(1-2\lambda) . \quad (27)$$

As mentioned earlier, they only contribute at NLL level.

Finally, following Eq. (10), we have expanded the hard-scattering functions $C_{ab}(\hat{\eta}, \alpha_s)$ in Eq. (20) to first order in α_s . As was pointed out in [9, 11], the inclusion of the $C_{ab}^{(1)}$ terms is significant, since with their help *three* towers of logarithms, $\alpha_s^n \ln^m(N)$, $2n-2 \leq m \leq 2n$, are brought under control in Eqs. (9), (20). In this way, the factors C_{ab} also help reduce the dependence of the cross section on the renormalization scale μ_R .

4 The hard-scattering functions $C_{ab}^{(1)}$

Expanding the expressions above in α_s , and comparing them to the exact NLO calculation of [17], we are able to check that indeed the logarithms of the type $\alpha_s \ln^2(N)$ and $\alpha_s \ln(N)$, which appear at NLO, are correctly reproduced by the resummation calculation, including their rapidity dependence [11]. This comparison also determines the explicit expressions for the N -independent coefficients $C_{ab}^{(1)}(\hat{\eta})$. For the $q\bar{q}$ annihilation process, we find:

$$\begin{aligned}
C_{q\bar{q}}^{(1)}(\hat{\eta}) = & \frac{1}{96} C_{q\bar{q}}^{(0)}(\hat{\eta}) \left\{ 12C_F \left(2 \ln[v(1-v)] (1 + \ln[v(1-v)]) - 4\rho_{q\bar{q}} \ln \left[\frac{Q^2}{2\mu_F^2 v(1-v)} \right] \right. \right. \\
& \left. \left. - 4 \ln v \ln(1-v) + \frac{20}{3}\pi^2 + \rho_{q\bar{q}}^2 + 6\rho_{q\bar{q}} - 19 \right) \right. \\
& - C_A \left(12(1 + \rho_{q\bar{q}}) \ln[v(1-v)] + 24 \left(\ln v \ln(1-v) + \pi^2 \right) + 3\rho_{q\bar{q}}^2 + 18\rho_{q\bar{q}} - 5 \right) \\
& + 8\pi b_0 \left(29 + 3\rho_{q\bar{q}} - 12 \ln \left[\frac{Q^2}{2\mu_R^2 \sqrt{v(1-v)}} \right] \right) \right\} \\
& + \frac{\pi e_q^2 C_F}{C_A} v(1-v) \left\{ -(C_A - 2C_F)(1+2v) \ln^2 v - 2C_A \ln v + 2C_F(5-6v) \ln v \right. \\
& \left. + (v \longleftrightarrow 1-v) \right\}, \tag{28}
\end{aligned}$$

where

$$\begin{aligned}
v &= 1 + \frac{t}{s} = \frac{e^{\hat{\eta}}}{2 \cosh \hat{\eta}} \\
\rho_{q\bar{q}} &= -3 + 4\gamma_E + 2 \ln[4v(1-v)]. \tag{29}
\end{aligned}$$

For qg QCD Compton scattering, one has:

$$\begin{aligned}
C_{qg}^{(1)}(\hat{\eta}) = & \frac{1}{4} C_{qg}^{(0)}(\hat{\eta}) \left\{ C_F \left(4 \ln^2 \frac{1-v}{v} + 2(\ln v - 3) \ln v - \rho_{qg}^{(F)} \ln \left[\frac{Q^2}{2\mu_F^2(1-v)} \right] \right. \right. \\
& \left. \left. + \frac{1}{8} (\rho_{qg}^{(F)})^2 + \frac{3}{2}\rho_{qg}^{(F)} + \frac{11}{3}\pi^2 - \frac{29}{8} \right) \right. \\
& - C_A \left(\ln^2 \frac{1-v}{v} + \rho_{qg}^{(A)} \ln \left[\frac{Q^2}{2\mu_F^2 v^2} \right] - \frac{1}{4} (\rho_{qg}^{(A)})^2 + \frac{1}{3}\pi^2 \right) - 4\pi b_0 \ln \left[\frac{\mu_F^2}{\mu_R^2} \right] \right\} \\
& + \frac{\pi e_q^2}{C_A} v^2 (1-v) \left\{ (C_A - 2C_F) \left[(3-2v) \left(\ln^2 \frac{1-v}{v} + \pi^2 \right) + (1-2v) \ln^2 v \right. \right. \\
& \left. \left. + 2(1-v) \ln \frac{1-v}{v^2} \right] + 6C_F \ln(1-v) \right\}, \tag{30}
\end{aligned}$$

where

$$\begin{aligned}
\rho_{qg}^{(F)} &= -3 + 4(\gamma_E + \ln[2v]) \\
\rho_{qg}^{(A)} &= 4(\gamma_E + \ln[2(1-v)]). \tag{31}
\end{aligned}$$

The values of the ratios $C_{ab}^{(1)}(\hat{\eta})/C_{ab}^{(0)}(\hat{\eta})$ at $\hat{\eta} = 0$ (that is, at $v = 1/2$) agree with the corresponding expressions in [9]. Despite the somewhat complicated rapidity dependence of the $C_{ab}^{(1)}$, it is possible to evaluate the integral in the last line of Eq. (20) in closed form. These results are given in Appendix B and complete the derivation of the resummed photon cross section in Mellin- N and Fourier space. We note that the explicit γ_E -terms of the coefficients, in Eqs. (29) and (31), as well as in $g_{ab}^{(2)}$ in Eqs. (23) and (24), can be eliminated [19] by redefining $\lambda = \alpha_s b_0 (\ln N e^{\gamma_E}) \equiv \alpha_s b_0 \ln \bar{N}$. This convention was adopted in Ref. [14].

5 The rapidity-integrated resummed cross section

We now compare to the calculation presented in [9], which aimed at threshold resummation of the η -integrated cross section. According to Eq. (3), integration over η is equivalent to setting $M = 0$ in our expressions and multiplying by $\sqrt{2\pi}$. We then find from (3), (7), (20) for the resummed cross section:

$$\begin{aligned} & \int_{-\infty}^{\infty} d\eta \int_0^{1/\cosh^2 \eta} dx_T^2 (x_T^2)^{N-1} \frac{p_T^3 d\sigma}{dp_T d\eta} \\ &= \alpha \alpha_s \sum_{a,b} \tilde{\phi}_a^{N+1} \tilde{\phi}_b^{N+1} \exp \left[\ln \tilde{N} g_{ab}^{(1)}(\tilde{\lambda}) + g_{ab}^{(2)}(\tilde{\lambda}) \right] \int_{-\infty}^{\infty} d\hat{\eta} (\cosh \hat{\eta})^{-2N+g_{ab}^{(3)}(\tilde{\lambda})} \left[C_{ab}^{(0)}(\hat{\eta}) + \frac{\alpha_s}{\pi} C_{ab}^{(1)}(\hat{\eta}) \right], \end{aligned} \quad (32)$$

to be compared to the result of [9], which can be written as

$$\begin{aligned} & \int_{-\infty}^{\infty} d\eta \int_0^{1/\cosh^2 \eta} dx_T^2 (x_T^2)^{N-1} \frac{p_T^3 d\sigma}{dp_T d\eta} \\ &= \alpha \alpha_s \sum_{a,b} \tilde{\phi}_a^{N+1} \tilde{\phi}_b^{N+1} \exp \left[\ln \tilde{N} g_{ab}^{(1)}(\tilde{\lambda}) + g_{ab}^{(2)}(\tilde{\lambda}) \right] \left[1 + \frac{\alpha_s}{\pi} \frac{C_{ab}^{(1)}(0)}{C_{ab}^{(0)}(0)} \right] \int_{-\infty}^{\infty} d\hat{\eta} (\cosh \hat{\eta})^{-2N} C_{ab}^{(0)}(\hat{\eta}). \end{aligned} \quad (33)$$

The two results become identical if the resummed exponent and the first-order correction in C_{ab} in Eq. (32) are evaluated at $\hat{\eta} = 0$, instead of retaining their full $\hat{\eta}$ dependence. We note from (32), however, that for large N the integrand is indeed strongly dominated by the region $\hat{\eta} \approx 0$. Therefore, setting $C_{ab}^{(1)}(\hat{\eta})/C_{ab}^{(0)}(\hat{\eta}) = C_{ab}^{(1)}(0)/C_{ab}^{(0)}(0)$ and neglecting the term proportional to $g_{ab}^{(3)}$ is expected to be a good approximation, and we anticipate that the two resummation formalisms should yield numerically very similar results for the η -integrated resummed cross section. On the other hand, if one wants to obtain fully consistent resummed results at fixed rapidity, one needs to make use of the full expression in Eq. (20) resulting from the formalism of [9].

6 Inverse transforms

The final step is to insert the result in Eq. (20) back into (7), and to take the Mellin and Fourier inverse transforms of $\sigma(N, M)$, in order to arrive at the physical hadronic cross section:

$$\begin{aligned}
\frac{p_T^3 d\sigma}{dp_T d\eta} &= \frac{1}{\sqrt{2\pi}} \int_{-\infty}^{\infty} dM e^{-iM\eta} \frac{1}{2\pi i} \int_{C-i\infty}^{C+i\infty} dN (x_T^2)^{-N} \sigma(N, M) \\
&= \frac{\alpha\alpha_s}{2\pi} \int_{-\infty}^{\infty} dM e^{-iM\eta} \frac{1}{2\pi i} \int_{C-i\infty}^{C+i\infty} dN (x_T^2)^{-N} \sum_{a,b} \tilde{\phi}_a^{N+1+\frac{iM}{2}} \tilde{\phi}_b^{N+1-\frac{iM}{2}} \\
&\quad \times \exp \left[\ln \tilde{N} g_{ab}^{(1)}(\tilde{\lambda}) + g_{ab}^{(2)} \left(\tilde{\lambda}, \frac{Q^2}{\mu_R^2}; \frac{Q^2}{\mu_F^2} \right) \right] \\
&\quad \times \int_{-\infty}^{\infty} d\hat{\eta} e^{iM\hat{\eta}} (\cosh \hat{\eta})^{-2N+g_{ab}^{(3)}(\tilde{\lambda})} \left[C_{ab}^{(0)}(\hat{\eta}) + \frac{\alpha_s}{\pi} C_{ab}^{(1)}(\hat{\eta}) \right], \tag{34}
\end{aligned}$$

where for the second equality we have made use of Eqs. (7) and (20), and where the last integral is given explicitly in Appendix B, as discussed above. Care has to be taken when choosing the contour in complex N space. First of all, the functions $g_{ab}^{(i)}(\lambda)$ have cut singularities starting at $\lambda = \frac{1}{2}$, that is, at $N = N_L = \exp(1/2b_0\alpha_s(\mu_R^2))$. These singularities result from the sensitivity of the original resummed expression (9) to the Landau pole [20], and signal the onset of non-perturbative phenomena very close to threshold. With the “minimal prescription” [10, 16] for the exponents given in Eqs. (21)-(26) above, we choose the constant C in (34) so that all singularities in the integrand are to the left of the integration contour, except for the Landau singularity at $N = N_L$, which lies to the far right. The contour is then deformed [10, 16, 21] into the half-plane with negative real part, which improves convergence while retaining the perturbative expansion. In this deformation, we need to avoid the moment-space singularities of the parton densities, which are displaced parallel to the imaginary axis by $\pm M/2$, as seen from Eq. (7). Thus, the intersection at C of the contour with the real axis has to lie far enough to the right that the contour does not pass through or below the singularities of the parton densities. At the same time, one can make the bending angle κ close to 90° to prevent this from happening. Our parameterization of the contour is given as

$$\begin{aligned}
N &= C + z e^{\pm i\kappa}, \quad (0 \leq z \leq \infty), \\
\kappa &= \pi - \arctan \left(\frac{C - 1 + M/2}{C - 1} \right). \tag{35}
\end{aligned}$$

The situation is depicted in Fig. 1.

7 Numerical results

For our numerical calculations, we use the NLO parton densities of [22]. The evolution code of [22] is set up in Mellin- N moment space and is therefore ideally suited for implementing the

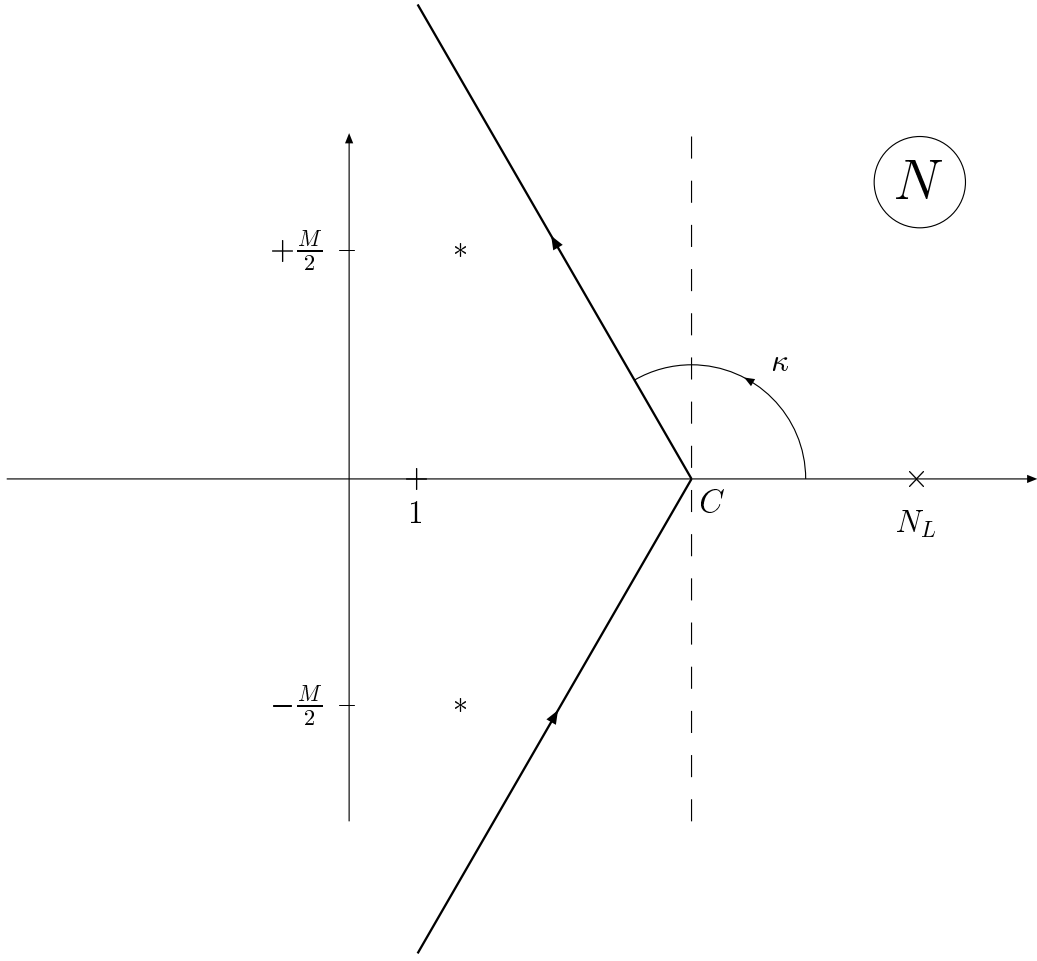


Figure 1: Contour in Mellin- N space for inverting the resummed cross section. The asterisks denote the rightmost poles of the parton densities which have acquired an imaginary part through the Fourier transformation in rapidity. N_L is the position of the Landau pole; see text.

resummation formulas in the way we have outlined above. In order to avoid double-counting of higher-order corrections, we subtract from the resummed expression (9) its perturbative expansion to $\mathcal{O}(\alpha_s)$, and subsequently add back in the full “exact” NLO prompt photon cross section [10]. For the latter, we use the calculation and the numerical code of [17] and also include an NLO fragmentation component, computed using the results of [23], along with the NLO photon fragmentation functions of [24]. Note that complete consistency would demand to also take into account the effects of threshold resummation on the fragmentation component [10, 14]. To mimic the expected effects, we multiply the NLO fragmentation component by the same factor by which the non-fragmentation part is changed through threshold resummation. Fortunately, the fragmentation contribution to the cross section is generally at the level of only 15 – 20%

anyway [5, 10], so the uncertainty residing here is not really crucial.

As in [10, 11], we will focus our calculations on the fixed-target region, where the observed disagreement of data and NLO theory calculations is largest, and which also is known [10, 11] to be generally more susceptible to threshold resummation effects than the collider regime, where the relevant values of x_T are much smaller. Figure 2 compares our results for the p_T dependence of the resummed prompt photon cross section with those of [10]. We use the same parton distribution functions [22] and rescaled fragmentation contribution for both curves¹. We show $E_\gamma d^3\sigma/dp_\gamma^3$, calculated for p-N collisions at $E_{\text{beam}} = 530$ GeV, corresponding to the Fermilab E706 fixed-target experiment [3], whose data are also displayed. We have chosen the scales $\mu_F = \mu_R = p_T$ and integrated over the rapidity range $|\eta| \leq 0.75$ accessed in the E706 experiment [3]. For better visibility, we have normalized all cross sections by the NLO one. One notices first of all that threshold resummation induces large effects at high p_T , where it leads to a sizeable enhancement of the theory prediction [10, 11], but is unimportant at the low- p_T end. Figure 2 also shows that there are only small differences between the results given by the two resummation formalisms. These have two origins: first, they are related to the neglect of the rapidity dependence in the resummation exponent and in the higher-order terms of the N -independent coefficients C_{ab} in [9]. As mentioned above, these differences would even be there, had we integrated over *all* kinematically allowed η , that is, over $|\eta| \leq \ln \left[\left(1 + \sqrt{1 - x_T^2} \right) / x_T \right]$. Second, since rapidity dependence in resummation was not available in [10], the means to compare to experimental data covering only a limited range of rapidity was to apply the following acceptance correction to the resummed cross section:

$$\sigma^{(\text{res})}(|\eta| \leq 0.75) \equiv \sigma^{(\text{res})}(\text{all } \eta) \frac{\sigma^{(\text{NLO})}(|\eta| \leq 0.75)}{\sigma^{(\text{NLO})}(\text{all } \eta)}. \quad (36)$$

That is, it was assumed that rescaling the η -integrated resummed cross section by an appropriate ratio of NLO cross sections correctly reproduces its rapidity dependence. This assumption of similarity of the resummed and NLO η -shapes is actually a fairly good approximation, as we will see below. We conclude from Fig. 2 that retaining the rapidity dependence in resummation induces very mild overall corrections for a cross section that is integrated over a substantial region including $\eta = 0$. As is evident from Figure 2, threshold resummation effects, albeit sizable in certain kinematic regions, are not sufficient to obtain a satisfactory description of the E706 data. This conclusion was first drawn in Refs. [10, 11].

We now turn to the rapidity dependence of the threshold-resummed cross section, where using the full formalism of [8] presented above is mandatory. The UA6 collaboration has presented data for the prompt photon cross section as a function of η , taken in pp and $\bar{p}p$ fixed-target scattering at $\sqrt{S} = 24.3$ GeV [4]. The transverse momentum of the photon was averaged over $4.1 < p_T < 7.7$ GeV. In Fig. 3 we compare our calculations to these data. In both plots,

¹The precise treatment of fragmentation and the choice of parton densities is different than in [10]. These choices have little numerical effect, however.

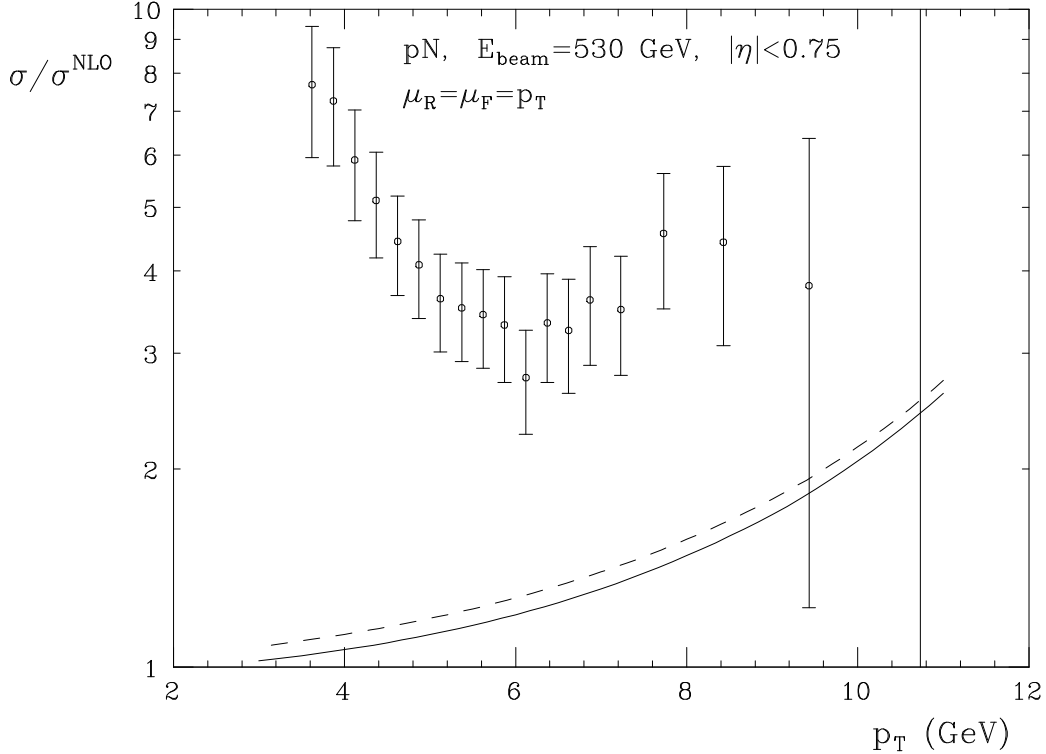


Figure 2: Threshold-resummed prompt photon cross sections, normalized to NLO, based on the formalisms of [9] (dashed) and [8] (solid). The parton densities were taken from [22]. The E706 prompt photon data [3] are also shown in the same normalization.

the dashed lines display the fixed-order NLO cross sections for three different choices of the renormalization and factorizations scales, $\mu_F = \mu_R = 2p_T, p_T, p_T/2$, from lower to upper. As can be seen, the variation of the NLO predictions induced by scale changes is very large, indicating the importance of yet higher-order effects. The solid lines in Fig. 3 show the results after adding in the effects of NLL threshold resummation. The most striking feature is a strong reduction of scale dependence. This effect was also found for the η -integrated cross section in [10]; our results demonstrate that it occurs over the whole η range. A closer analysis reveals that the main reduction in scale dependence is associated with the factorization scale. The reasons for this were discussed in [13, 25]. Also, the scale dependence decreases even further if we push our calculation to larger x_T . Both these observations are corroborated by Fig. 4, where we return to the conditions of the E706 experiment [3], looking at the rapidity dependence of the cross section at a fixed, high, photon transverse momentum $p_T = 10$ GeV. The dashed lines again show the NLO cross section for three choices of scales, $\mu_F = \mu_R = 2p_T, p_T, p_T/2$, and the solid lines display their resummed counterparts. Clearly, the reduction in scale dependence after resummation is dramatic here. The dotted lines in Fig. 4 refer to the NLO cross section for fixed renormalization scale $\mu_R = p_T$, but varying the factorization scale in the range used previously. The scale

dependence of the NLO cross section thus mainly is due to that on μ_F , and the improvement in μ_F dependence after resummation, shown by the dot-dashed lines, is striking.

We note that resummation of the η -dependence of the cross section was also considered in [11]. There the resummed expression was expanded to $\mathcal{O}(\alpha_s^2)$, thus testing the effects of the NNLO terms generated by resummation. The numerical results of [11] indeed also show some reduction in scale dependence which, however, is not as substantial as the one we find. This implies that resummation effects beyond NNLO are still important, and that the full resummed series should be taken into account. Our examples in Figs. 3, 4 also show that threshold resummation mainly affects the normalization of the cross section, and less so its shape in η for moderate η . Nevertheless, as we now show, large rapidity can, like high p_T , enhance resummation effects.

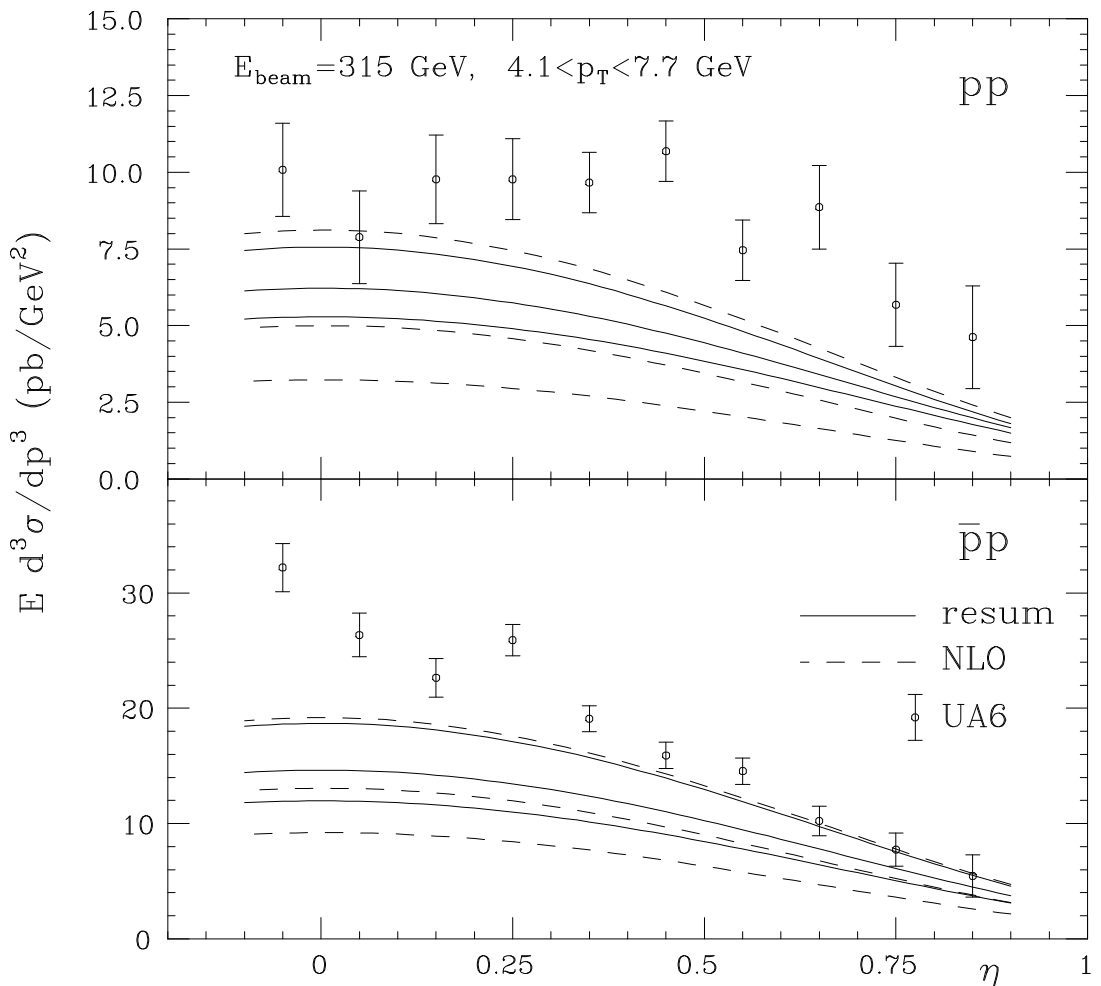


Figure 3: Rapidity dependence of the prompt photon cross section in pp and $\bar{p}p$ collisions at $\sqrt{S} = 24.3$ GeV. Dashed lines are NLO, solid lines denote the cross section resummed to NLL accuracy. For each case, the results have been calculated for three choices of scales, $\mu_F = \mu_R = 2p_T, p_T, p_T/2$, from lower to upper. The data are from UA6 [4].

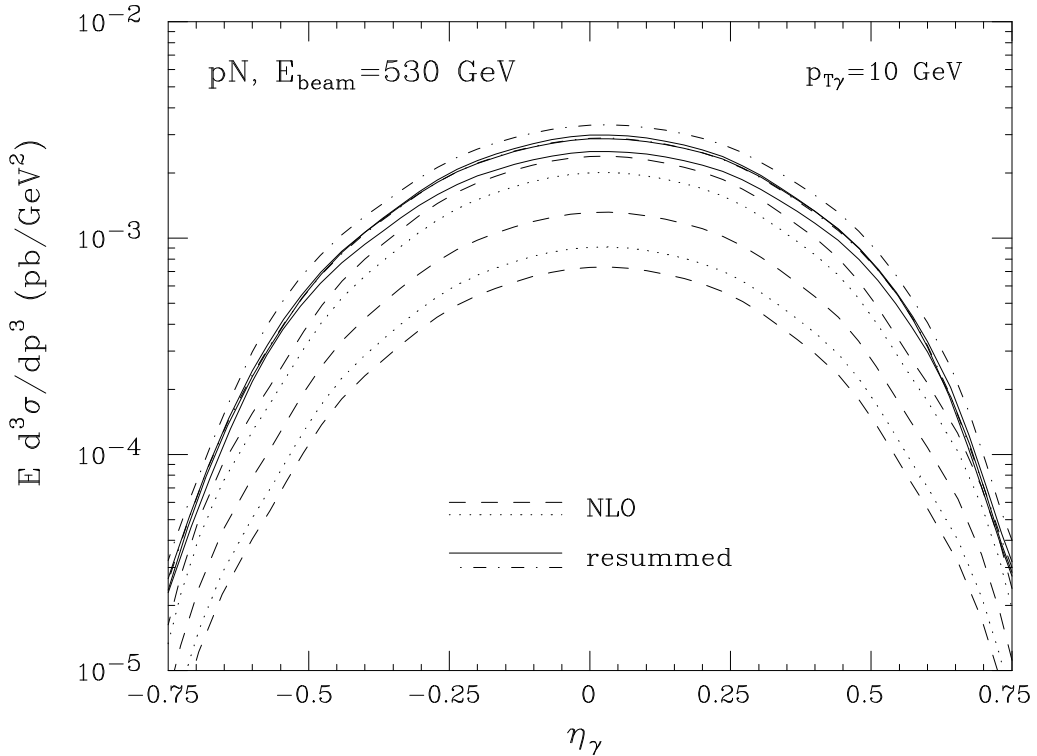


Figure 4: Rapidity dependence of the prompt photon cross section in pN collisions at $\sqrt{S} = 31.5$ GeV. Dashed and dotted lines are NLO, solid and dot-dashed lines denote the cross section resummed to NLL accuracy. For each case, the results have been calculated for five choices of scales, $\mu_F = \mu_R = 2p_T, p_T, p_T/2$ (dashed and solid), and $\mu_F = 2p_T, p_T/2$ at fixed $\mu_R = p_T$ (dotted and dot-dashed), from lower to upper.

We have mentioned earlier that threshold resummation for the prompt photon cross section is typically expected to be relevant in the fixed-target regime, but less so for collider energies, where a given x_T implies a much larger value of p_T and hence a much smaller cross section. As a result, the highest- p_T prompt photons seen at the Tevatron are at around $p_T \approx 100$ GeV [2], where $x_T \approx 0.1$ which is too small for threshold effects to be really important. However, we can ask what the effects of threshold resummation would be, *were* we able to go out in p_T to, say, $p_T = 500$ GeV. Keeping in mind that the Tevatron jet data [26] do reach out to p_T 's of that size, this question becomes of some relevance, provided threshold resummation effects for the prompt photon cross section have any resemblance to those for the jet cross section. Fig. 5 shows a calculation of threshold resummation effects on the cross section for very-high- p_T prompt photons, produced in $p\bar{p}$ collisions at $\sqrt{S} = 1800$ GeV. The results are normalized to the corresponding NLO cross section. The solid line shows the cross section averaged over $|\eta| < 0.9$, used for the actual CDF prompt photon data [2], whereas the dashed and dotted lines present the result at a fixed near-central ($\eta = 0.7$) and forward ($\eta = 1.4$) rapidity, respectively. It is evident that at such high p_T threshold resummation effects are sizable even at collider energy, and that,

at a given p_T , they tend to become more important with increasing $|\eta|$, that is, toward the limit of phase space where large momentum fractions in the parton densities are probed. At low η , effects remain modest even at large p_T , as recently observed directly in an NNLO expansion [27] of the resummed jet cross section. Our finding could be indicative of significant effects also for jet production at the Tevatron, in particular in the off-central region. This result is also suggestive of recent data [29] which hints at an excess of high- p_T jets that increases with η . This issue will bear further investigation.

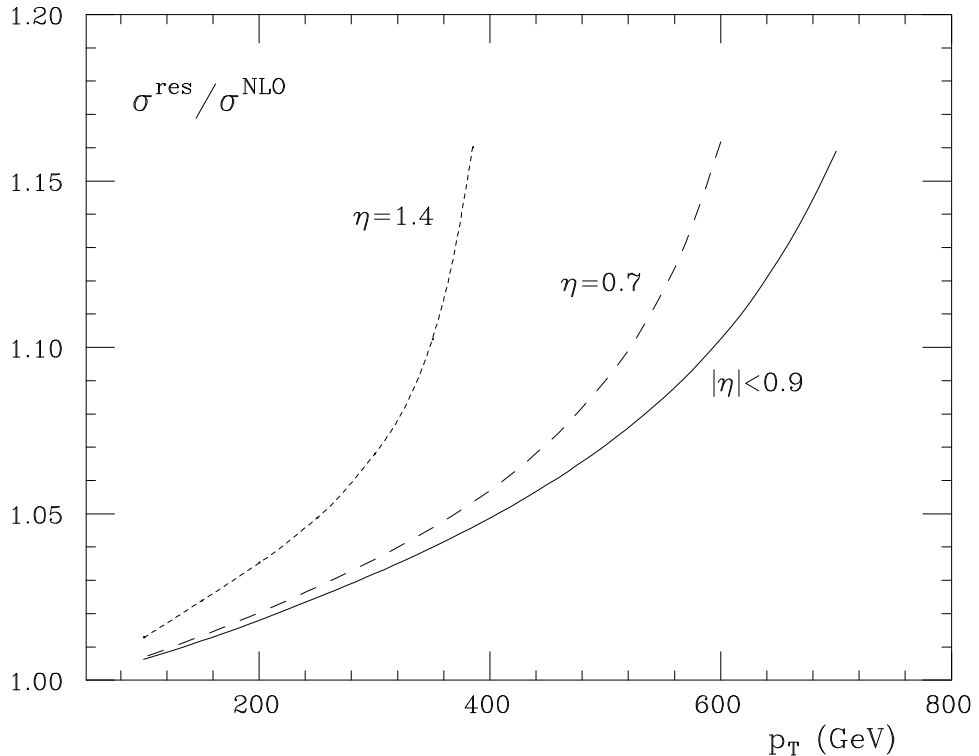


Figure 5: Threshold-resummed prompt photon cross sections, normalized to NLO, for $p\bar{p}$ collisions at $\sqrt{S} = 1800$ GeV.

Acknowledgments

We are grateful to S. Catani and N. Kidonakis for very valuable discussions. This work was supported in part by the National Science Foundation, grant PHY9722101. G.S. acknowledges the hospitality of Brookhaven National Laboratory. W.V. thanks RIKEN, Brookhaven National Laboratory and the U.S. Department of Energy (contract number DE-AC02-98CH10886) for providing the facilities essential for the completion of this work.

Appendix A

In this appendix we give explicit expansions of the exponents in Eq. (9) to NLL accuracy. These are analogous to the expressions given in Appendix A of Ref. [9]. We expand each of the functions $\mathcal{G}_i(\alpha_s) \equiv A_i(\alpha_s), \bar{B}_i(\dots, \alpha_s), \gamma_i(\alpha_s), \gamma_{ii}(\alpha_s), \text{Re}\Gamma_S^{(ab \rightarrow \gamma c)}(\hat{\eta}, \alpha_s)$ as a power series in α_s/π :

$$\mathcal{G}_i(\alpha_s) = \sum_{k=1}^{\infty} \left(\frac{\alpha_s}{\pi} \right)^k \mathcal{G}_i^{(k)}(\alpha_s) . \quad (37)$$

We then find

$$\begin{aligned} E_i(2N_i, M_i) &= \frac{1}{\alpha_s(\mu_R^2)} \mathcal{H}_i^{(0)}(\lambda_i) + \mathcal{H}_i^{(1)} \left(\lambda_i, \frac{M_i^2}{\mu_R^2}, \frac{M_i^2}{\mu_F^2} \right) - \frac{1}{2\pi b_0} \bar{B}_i^{(1)} \left(\nu_i, \frac{M_i^2}{s} \right) \ln(1 - 2\lambda_i) , \\ E'_i(2N, s) &= \frac{1}{\alpha_s(\mu_R^2)} \mathcal{F}_i^{(0)}(\lambda) + \mathcal{F}_i^{(1)} \left(\lambda, \frac{s}{\mu_R^2} \right) - \frac{1}{2\pi b_0} \bar{B}_i^{(1)}(\nu_i, 1) \ln(1 - 2\lambda) , \\ \int_{\mu_R}^{\sqrt{s}/2N} \frac{d\mu'}{\mu'} 2 \text{Re}\Gamma_S^{(ab \rightarrow \gamma c)} \left(\hat{\eta}, \alpha_s(\mu'^2) \right) &= \frac{\Gamma_S^{(ab \rightarrow \gamma c)(1)}(\hat{\eta})}{\pi b_0} \ln(1 - 2\lambda) , \end{aligned} \quad (38)$$

where $\lambda = \alpha_s(\mu_R^2)b_0 \ln N$, $\lambda_i = \alpha_s(\mu_R^2)b_0 \ln N_i$, and

$$\begin{aligned} \mathcal{H}_i^{(0)}(\lambda) &= \frac{A_i^{(1)}}{2\pi b_0^2} [2\lambda + (1 - 2\lambda) \ln(1 - 2\lambda)] , \\ \mathcal{H}_i^{(1)} \left(\lambda, \frac{M_i^2}{\mu_R^2}, \frac{M_i^2}{\mu_F^2} \right) &= \frac{A_i^{(1)} b_1}{2\pi b_0^3} \left[\frac{1}{2} \ln^2(1 - 2\lambda) + 2\lambda + \ln(1 - 2\lambda) \right] - \frac{A_i^{(1)}(\gamma_E + \ln 2)}{\pi b_0} \ln(1 - 2\lambda) \\ &\quad + \frac{1}{2\pi b_0} \left(-\frac{A_i^{(2)}}{\pi b_0} + A_i^{(1)} \ln \left(\frac{M_i^2}{\mu_R^2} \right) \right) [2\lambda + \ln(1 - 2\lambda)] - \frac{A_i^{(1)}}{\pi b_0} \lambda \ln \left(\frac{M_i^2}{\mu_F^2} \right) , \\ \mathcal{F}_i^{(0)}(\lambda) &= 2\mathcal{H}_i^{(0)}(\lambda/2) - \mathcal{H}_i^{(0)}(\lambda) , \\ \mathcal{F}_i^{(1)}(\lambda) &= 2\mathcal{H}_i^{(1)}(\lambda/2) - \mathcal{H}_i^{(1)}(\lambda) + \frac{1}{\pi b_0} [A_i^{(1)}(\gamma_E + \ln 2) - \gamma_i^{(1)}] \ln(1 - \lambda) . \end{aligned} \quad (40)$$

To NLL accuracy, we further expand

$$\ln(1 - 2\lambda_i) \approx \ln(1 - 2\lambda) - \frac{2 \alpha_s(\mu_R^2) b_0}{1 - 2\lambda} \ln(N_i/N) , \quad (41)$$

where we recall that $N_a/N = -u/s$, $N_b/N = -t/s$. From the appropriate sums of these expressions, the $g_{ab}^{(i)}$'s of Eqs. (21)-(27) are identified through the linear dependence on $\ln N$ and $\ln(\cosh \hat{\eta})$.

Appendix B

In this appendix, we exhibit the $\hat{\eta}$ -integrals of Eq. (20) for the coefficients $C_{ab}^{(0,1)}(\hat{\eta})$ of Eqs. (11), (28), (30). After substitution $x \equiv \exp(2\hat{\eta})$, one is led to integrals of the type

$$P_{c,d}(a, b) \equiv 2^{-2-b} \int_0^\infty dx x^a (1+x)^b \ln^c x \ln^d(1+x) \quad (c, d \in \{0, 1, 2\}) , \quad (42)$$

which can be expressed in terms of the Γ function and its derivatives:

$$\begin{aligned} P_{0,0}(a, b) &= \frac{1}{2} B\left(\frac{1}{2}, -\frac{b}{2}\right) \frac{\Gamma(a+1)\Gamma(-a-b-1)}{\Gamma^2(-b/2)} , \\ P_{1,0}(a, b) &= P_{0,0}(a, b) [\psi(a+1) - \psi(-a-b-1)] , \\ P_{0,1}(a, b) &= P_{0,0}(a, b) [\psi(-b) - \psi(-a-b-1)] , \\ P_{2,0}(a, b) &= P_{0,0}(a, b) [\psi'(a+1) + \psi'(-a-b-1)] + [P_{1,0}(a, b)]^2 / P_{0,0}(a, b) , \\ P_{0,2}(a, b) &= P_{0,0}(a, b) [\psi'(-a-b-1) - \psi'(-b)] + [P_{0,1}(a, b)]^2 / P_{0,0}(a, b) , \\ P_{1,1}(a, b) &= P_{0,0}(a, b) \psi'(-a-b-1) + P_{1,0}(a, b) P_{0,1}(a, b) / P_{0,0}(a, b) , \end{aligned} \quad (43)$$

where $\psi(z) \equiv d \ln \Gamma(z) / dz$ and $\psi'(z) \equiv d\psi(z) / dz$. The numerical treatment of these functions for complex arguments was discussed in [28]. For convenience, we also abbreviate

$$\begin{aligned} R_{i,j}(a, b) &\equiv P_{i,j}(a, b) + P_{i,j}(a+2, b) , \\ S_{i,j}(a, b) &\equiv 2P_{i,j}(a, b) + 2P_{i,j}(a+1, b) + P_{i,j}(a+2, b) . \end{aligned} \quad (44)$$

We then have for $q\bar{q}$ scattering:

$$\begin{aligned} &\int_{-\infty}^\infty d\hat{\eta} e^{iM\hat{\eta}} (\cosh \hat{\eta})^{-2N+g_{q\bar{q}}^{(3)}(\tilde{\lambda})} \left[C_{q\bar{q}}^{(0)}(\hat{\eta}) + \frac{\alpha_s}{\pi} C_{q\bar{q}}^{(1)}(\hat{\eta}) \right] \\ &= \frac{C_F \pi}{C_A} e_q^2 \left\{ R_{0,0}(a, b) \left(1 + \frac{\alpha_s}{\pi} \left[(2C_F - C_A/2) (\gamma_E^2 + 2\zeta(2)) + \pi b_0 (\gamma_E + 2 \ln 2) \right. \right. \right. \\ &\quad \left. \left. \left. + (6C_F - C_A) \gamma_E \ln 2 - \frac{3}{2} C_F \ln 2 + (4C_F - C_A/2) \ln^2 2 \right. \right. \right. \\ &\quad \left. \left. \left. + K/2 - K_q - C_F (2\gamma_E + 2 \ln 2 - 3/2) \ln \frac{Q^2}{\mu_F^2} - \pi b_0 \ln \frac{Q^2}{\mu_R^2} \right] \right) \\ &\quad + \frac{\alpha_s}{\pi} \left\{ -\frac{3}{2} C_F R_{0,1}(a, b) - \frac{1}{4} (R_{2,0}(a, b) + 3R_{0,2}) (3C_A - 10C_F) + \frac{1}{2} R_{1,1}(a, b) (5C_A - 16C_F) \right. \\ &\quad + (R_{1,0}(a, b) - 2R_{0,1}(a, b)) \left(-\frac{3}{2} C_F + (4C_F - C_A) \gamma_E + \pi b_0 - C_F \ln \frac{Q^2}{\mu_F^2} + (5C_F - C_A) \ln 2 \right) \\ &\quad + \frac{3}{2} C_F P_{1,0}(a, b) + \frac{1}{4} (C_A - 2C_F) (-2P_{1,0}(a+1, b) + 4P_{0,1}(a+1, b) + P_{2,0}(a, b) \\ &\quad \left. \left. - 2P_{2,0}(a+1, b) - 4P_{0,2}(a+1, b) - 2P_{1,1}(a, b) + 4P_{1,1}(a+1, b) \right) \right\} \right\} , \end{aligned} \quad (45)$$

where

$$\begin{aligned}
K_q &= \left(\frac{7}{2} - \zeta(2) \right) C_F, \\
a &= N - g_{q\bar{q}}^{(3)}(\tilde{\lambda})/2 + iM/2, \\
b &= -2N + g_{q\bar{q}}^{(3)}(\tilde{\lambda}) - 4.
\end{aligned} \tag{46}$$

The coefficient K has already been defined in Eq. (13). For qg scattering, we find:

$$\begin{aligned}
& \int_{-\infty}^{\infty} d\hat{\eta} e^{iM\hat{\eta}} (\cosh \hat{\eta})^{-2N+g_{qg}^{(3)}(\tilde{\lambda})} \left[C_{qg}^{(0)}(\hat{\eta}) + \frac{\alpha_s}{\pi} C_{qg}^{(1)}(\hat{\eta}) \right] \tag{47} \\
&= \frac{\pi}{4C_A} e_q^2 \left\{ S_{0,0}(a, b) \left(1 + \frac{\alpha_s}{\pi} \left[(C_A + C_F/2)\gamma_E^2 - \frac{1}{2}K_q + (C_A + 2C_F)\zeta(2) + (2C_A + 3C_F/2)\ln^2 2 \right. \right. \right. \\
& \quad \left. \left. \left. + (3C_A + 2C_F)\gamma_E \ln 2 + \pi b_0 \ln \frac{\mu_R^2}{\mu_F^2} + \frac{3}{4}C_F \left(\gamma_E + \ln \frac{Q^2}{\mu_F^2} \right) - (C_A + C_F)(\gamma_E + \ln 2) \ln \frac{Q^2}{\mu_F^2} \right] \right) \right. \\
& \quad + \frac{\alpha_s}{\pi} \left\{ S_{1,0}(a, b) \left(-\frac{3}{4}C_F + (2C_A + C_F)\gamma_E + 2(C_A + C_F) \ln 2 - C_F \ln \frac{Q^2}{\mu_F^2} \right) \right. \\
& \quad \left. - S_{0,1} \left(2(2C_A + C_F)\gamma_E + (5C_A + 3C_F) \ln 2 - (C_A + C_F) \ln \frac{Q^2}{\mu_F^2} \right) + \frac{1}{2}(C_A + C_F)P_{0,1}(a, b) \right. \\
& \quad - \frac{1}{4}(C_A - 8C_F)S_{2,0}(a, b) + \frac{1}{4}(11C_A + 10C_F)S_{0,2}(a, b) - \frac{1}{2}(3C_A + 8C_F)S_{1,1}(a, b) \\
& \quad + \frac{1}{4}(C_A - 2C_F) \left((P_{0,0}(a, b) + 2P_{0,0}(a+1, b))\pi^2 - 4P_{1,0}(a, b) - 4P_{1,0}(a+1, b) + 2P_{0,1}(a+1, b) \right. \\
& \quad \left. \left. + 4P_{2,0}(a, b) + 4P_{2,0}(a+1, b) + 3P_{0,2}(a, b) + 2P_{0,2}(a+1, b) - 6P_{1,1}(a, b) - 4P_{1,1}(a+1, b) \right) \right\} ,
\end{aligned}$$

where in this case

$$\begin{aligned}
a &= N - g_{qg}^{(3)}(\tilde{\lambda})/2 + 1 + iM/2, \\
b &= -2N + g_{qg}^{(3)}(\tilde{\lambda}) - 5.
\end{aligned} \tag{48}$$

It is evident from Eq. (43) that when performing the $\hat{\eta}$ integrations one inevitably introduces non-leading contributions in the moment variable N . This is already true when keeping only the Born approximations $C_{ab}^{(0)}(\hat{\eta})$ for the hard scattering, and is not in conflict with the approximations made in threshold resummation, where the resummed exponents are always convoluted with smooth functions, like the parton densities, that abundantly contain terms subleading in N . We note that for large N the one-loop parts of Eqs. (45), (47) converge to the respective coefficients given in Eqs. (58), (59) of [9] for the case of the η -integrated cross section, as they must.

References

- [1] For a review of the prompt photon data, see: W. Vogelsang and M. Whalley, J. Phys. **G23** (1997) A1.
- [2] F. Abe et al., CDF Collab., Phys. Rev. Lett. **73** (1994) 2662; S. Kuhlmann, et al., CDF Collab., Nucl. Phys. Proc. Suppl. **79** (1999) 241; B. Abbott et al., D0 Collab., Phys. Rev. Lett. **84** (2000) 2786.
- [3] L. Apanasevich et al., E706 Collab., Phys. Rev. Lett. **81** (1998) 2642.
- [4] G. Ballocchi et al., UA6 Collab., Phys. Lett. **B436** (1998) 222.
- [5] W. Vogelsang and A. Vogt, Nucl. Phys. **B453** (1995) 334.
- [6] J. Huston et al., Phys. Rev. **D51** (1995) 6139.
- [7] P. Aurenche, M. Fontannaz, J.-Ph. Guillet, B. Kniehl, E. Pilon and M. Werlen, Eur. Phys. J. **C9** (1999) 107.
- [8] E. Laenen, G. Oderda and G. Sterman, Phys. Lett. **B438** (1998) 173.
- [9] S. Catani, M.L. Mangano and P. Nason, JHEP **9807** (1998) 024.
- [10] S. Catani, M.L. Mangano, P. Nason, C. Oleari and W. Vogelsang, JHEP **9903** (1999) 025.
- [11] N. Kidonakis and J.F. Owens, Phys. Rev. **D61** (2000) 094004.
- [12] G. Sterman, Nucl. Phys. **B281** (1987) 310; S. Catani and L. Trentadue, Nucl. Phys. **B327** (1989) 323; **B353** (1991) 183; N. Kidonakis and G. Sterman, Nucl. Phys. **B505** (1997) 321.
- [13] R. Bonciani, S. Catani, M.L. Mangano and P. Nason, Nucl. Phys. **B529** (1998) 424.
- [14] E. Laenen, G. Sterman and W. Vogelsang, Phys. Rev. Lett. **84** (2000) 4296; [hep-ph/0010080](https://arxiv.org/abs/hep-ph/0010080).
- [15] H.-n. Li, Phys. Lett. **B454** (1999) 328.
- [16] S. Catani, M.L. Mangano, P. Nason and L. Trentadue, Nucl. Phys. **B478** (1996) 273.
- [17] L.E. Gordon and W. Vogelsang, Phys. Rev. **D48** (1993) 3136.
- [18] N. Kidonakis, G. Oderda and G. Sterman, Nucl. Phys. **B525** (1998) 299; Nucl. Phys. **B531** (1998) 365.
- [19] N. Kidonakis, [hep-ph/0010002](https://arxiv.org/abs/hep-ph/0010002).

- [20] S. Catani and L. Trentadue, Nucl. Phys. **B327** (1989) 323;
 S. Catani, L. Trentadue, G. Turnock and B.R. Webber, Nucl. Phys. **B407** (1993) 3.
- [21] H. Contopanagos and G. Sterman, Nucl. Phys. **B419** (1994) 77.
- [22] M. Glück, E. Reya and A. Vogt, Eur. Phys. J. **C5** (1998) 461.
- [23] F. Aversa, P. Chiappetta, M. Greco and J.-Ph. Guillet, Nucl. Phys. **B327** (1989) 105.
- [24] M. Glück, E. Reya and A. Vogt, Phys. Rev. **D48** (1993) 116, E: **D51** (1995) 1427.
- [25] G. Sterman and W. Vogelsang, in *High Energy Physics 99*, proceedings of the International Europhysics Conference on High-Energy Physics, ed. K. Huitu et al. (Institute of Physics Publishing, Bristol, UK, 2000), [hep-ph/9910371](#).
- [26] see, for example: L. Babukhadia, D0 Collab., talk given at the 35th Rencontres de Moriond: QCD and High Energy Hadronic Interactions, Les Arcs, France, March 2000, [hep-ex/0005026](#).
- [27] N. Kidonakis and J.F. Owens, [hep-ph/0007268](#).
- [28] M. Glück, E. Reya and A. Vogt, Z. Phys. **C48** (1990) 471.
- [29] V. D. Elvira et al., D0 Collab., [hep-ex/0010032](#).